Supporting information

Text S1. Materials and chemicals

Alkaline lignin, PMS ($KHSO_5 \cdot 0.5KHSO_4 \cdot 0.5K_2SO_4$), 2,2,6,6-tetramethylpiperidine (TEMP), 5,5-dimethyl-1-pyrroline N-oxide (DMPO), tert-butanol (TBA) were obtained from Aladdin Co. ltd., China. Cobaltous nitrate hexahydrate ($Co(NO_3)_2 \cdot 6H_2O$), methanol (MeOH), absolute ethanol (EtOH), furfuryl alcohol (FFA), p-Benzoquinone (p-BQ), hydrochloric acid (HCl), sulfuric acid (H_2SO_4), sodium chloride (NaCl), sodium dihydrogen phosphate (NaH_2PO_4), sodium hydroxide (NaOH), sodium hydrogen carbonate ($NaHCO_3$), sodium nitrate ($NaNO_3$), sodium sulfate (Na_2SO_4), humic acid (HA), norfloxacin (NOR), tetracycline (TC), oxytetracycline (OTC), ofloxacin (OFX), ciprofloxacin (CIP) were purchased from Sinopharm Chemical Reagent Co. ltd. All materials or chemicals used were of analytical purity grade and used without further purification.

Text S2. Material characterization

Morphology and microstructure of the samples were examined by scanning electron microscope (SEM, ZEISS Sigma 300) and transmission electron microscopy (TEM, FEI Tecnai G2 F20). The chemical groups were analyzed by Fourier transforms infrared (FTIR, Thermo Fisher Nicolet IS5). Crystal phases were analyzed by X-ray diffraction (XRD, BRUKER D8 ADVANCE). Raman spectra were acquired on a LabRAM HR Evolution spectrometer to evaluate the graphitization degree and defect density. Surface elemental composition and chemical states were analyzed by X-ray photoelectron spectroscopy (XPS, Thermo Fisher-Thermo Scientific K-Alpha). Nitrogen adsorption–desorption isotherms were measured at 77 K using a Micromeritics ASAP 2460 analyzer to determine specific surface area (BET method) and pore structure. Electron paramagnetic resonance (EPR) spectra were recorded on a Magnettech MS-5000 spectrometer using DMPO and TEMP as the trapping agents to detect •OH, $SO_4^{\bullet -}$, $O_2^{\bullet -}$, and $^1O_2$.

Text S3. Analytical methods

NOR concentration was quantified by high-performance liquid chromatography (HPLC, Agilent 1260) equipped with a ZORBAX SB-C18 column (250 × 4.6 mm, 5 μm); the mobile phase consisted

of methanol and 0.1% (v/v) phosphoric acid aqueous solution (30:70) at a flow rate of 1.0 mL/min, with UV detection at 278 nm. A three-dimensional fluorescence spectrophotometer (3D-EEM, F-7000, Hitachi, Japan) was used to monitor the fluorescence changes of NOR. Excitation wavelengths ranged from 200 to 500 nm (5 nm intervals), and emission wavelengths spanned 250 to 550 nm. The scan increment and slit widths were set to 5 nm and 10 nm for both excitation and emission, respectively. The scanning speed was 3000 nm/min, and the voltage of the photomultiplier tube was 650 V. The intermediates of NOR degradation were identified by liquid chromatography-mass spectrometry (LC-MS, Agilent LC1290) using an electrospray ionization (ESI) source in positive mode; mass spectra were acquired in the range of m/z 50-380. The mobile phase consisted of solvent A (acetonitrile) and solvent B (0.1% formic acid in water). The flow rate was 0.4 mL/min, and the injection volume was 5 μL.

Density functional theory (DFT) calculations were performed using the DMol3 module in Materials Studio. The molecular geometry of NOR was fully optimized in the gas phase using the generalized gradient approximation (GGA) with the Perdew-Burke-Ernzerhof (PBE) functional and a double numerical plus d-polarization (DNP) basis set. Based on the optimized structure, the electrostatic potential (ESP) mapped onto the electron density isosurface, the highest occupied molecular orbital (HOMO), the lowest unoccupied molecular orbital (LUMO), and the Fukui function for nucleophilic (f^-), electrophilic (f^+), and radical (f^0) attacks were calculated to evaluate the reactive sites of NOR toward different oxidative species.

Table S1. BET surface area, pore volume, and average pore diameter of different samples.

Samples	S^{a}_{BET} ($m^2 \cdot g^{-1}$)	V^{b}_{pore} ($cm^3 \cdot g^{-1}$)	$D_{pore\ size}$ (nm)
BC700	324.7	0.472	3.818
CoBC550	236.9	0.262	3.833
CoBC700	241.6	0.534	3.824
CoBC850	192.3	0.352	3.820
used CoBC700	96.2	0.298	3.837

[a] Calculated using the multi-point BET method.

[b] Total pore volume of pores at P/P_0=0.99.

Table S2. Cobalt loading amount in CoBC700 and cobalt leaching concentration in CoBC700/PMS system.

Sample	Cobalt loading (wt.%)	Cobalt leaching concentration (mg/L)
CoBC700	28.17	0.54

Table S3. Fukui function of NOR

Atom	f^+	f^-	f^0
1(C)	0.023	0.026	0.025
2(C)	0.033	0.023	0.028
3(C)	0.010	0.017	0.013
4(C)	0.013	0.007	0.010
5(C)	0.031	0.015	0.023
6(C)	0.046	0.034	0.040
7(C)	0.018	0.051	0.035
8(C)	0.043	0.009	0.026
9(C)	0.115	0.045	0.080
10(N)	0.039	0.033	0.036
11(C)	0.010	0.009	0.009
12(C)	0.008	0.007	0.008
13(O)	0.059	0.188	0.124
14(C)	0.057	0.043	0.050
15(O)	0.098	0.106	0.102
16(O)	0.042	0.058	0.050
17(F)	0.036	0.031	0.034
18(N)	0.024	0.030	0.027
19(C)	0.005	0.006	0.005
20(C)	0.004	0.004	0.004
21(N)	0.008	0.008	0.008
22(C)	0.005	0.005	0.005
23(C)	0.005	0.005	0.005

Figure S1. Pore size distributions of BC700 and CoBCx.

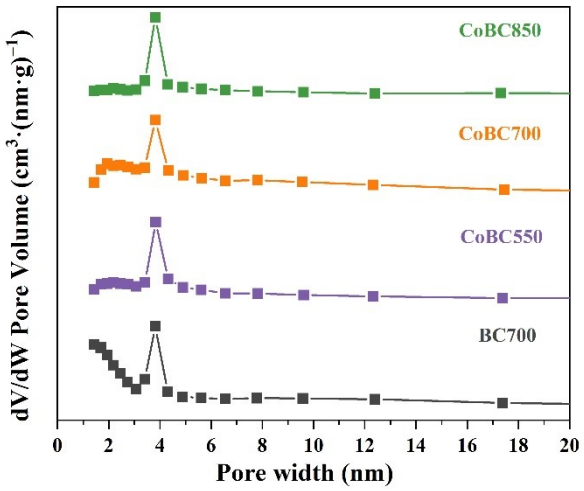

Figure S2. Effect of different cobalt doping amounts (a); Effect of CoBC700 dosage (b); Effect of PMS concentration (c) on NOR degradation; Effect of NOR concentration on the degradation (d).

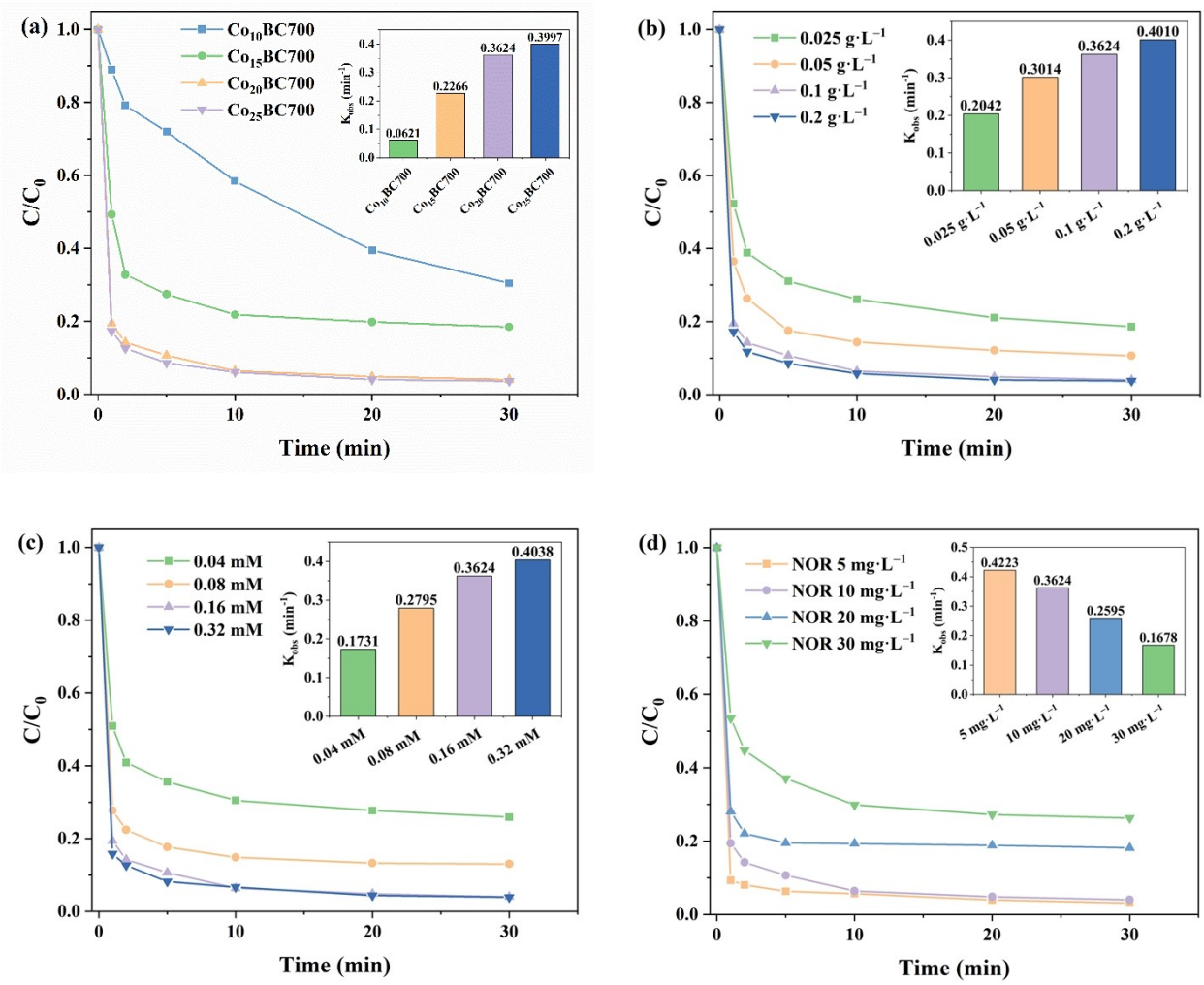

Figure S3. OCP of the CoBC700/PMS complex.